Point-to-Point Iterative Learning Control with Quantized Input Signal and Actuator Faults

ABSTRACT

This paper applies iterative learning control to point-to-point tracking problems with a general networked structure. The data is quantized and transmitted through restricted communication channels from the controller to the actuator. Combining a logarithmic quantizer with an encoding and decoding mechanism to quantize the input signals reduces the influence of the quantization error. New design algorithms are developed with conditions for convergence of the tracking error and an extension to fault-tolerant performance under actuator failures. A numerical-based case study demonstrates the application of the new designs, which includes a comparison with another ILC law and the relative merits of the encoding and decoding schemes.

1. Introduction

Iterative learning control (ILC) is a well-established research area for application to systems that repeatedly complete the same finite-duration task. Each execution of the task is commonly known as a trial, and the term trial length denotes the finite duration of a trial. Once each trial is complete, all information generated is available for use in computing the control input to be applied on the subsequent trial. In ILC design, a reference trajectory is specified, and the objective is to construct a sequence of trial inputs to improve performance from trial-to-trial sequentially.

In this paper, the nonnegative integer subscript k on variables denotes the trial number, and $0 \leq t \leq \alpha$ is the variable along a trial where $\alpha < \infty$ denotes the trial length (continuous or discrete dynamics along the trial are possible, where in the latter case the number of samples along the trial is often used instead of the trial length). Let $y_k(t)$ represent the output on trial k and $u_k(t)$ the input on this trial, where these variables can be vector or scalar-valued. Suppose that $y_d(t)$ is the reference trajectory. Then the error on trial k is $e_k(t) = y_d(t) - y_k(t)$ and the control design problem is to construct a sequence of control inputs $\{u_k\}_k$ such that $\{e_k\}_k$ converges. An appropriate norm measures convergence, and the objective is to force the output sequence to converge with k to zero or to within a specified tolerance.

Once a trial is complete, the system resets to the starting location. All information generated over $0 \leq t \leq \alpha$ is available to construct the control input to be applied on the subsequent trial. Hence in a common form of ILC law, the input for any trial is constructed as the sum of that used on the previous trial plus a correction term that

can use information from the previous complete trial data. Since the first work, widely credited to (Arimoto et al., 1984), ILC has been applied in many practical applications, such as chemical batch processes (Tao et al., 2017), robotics (Chen et al., 2019; Jin, 2018b), and wafer stage design (Oomen and Rojas, 2017).

ILC in healthcare applications is a significant area of research. For example, people with a stroke lose functionality down one side of their body and hence have an impaired ability to complete daily tasks, such as reaching out to an object over a tabletop. The recommended way, supported by the healthcare literature, is repeated attempts at the task where the error at the end of one attempt acts as feedback on improving performance on a subsequent attempt. The difficulty is that stroke patients have impaired functionality of the affected limb, i.e., in the ability to move the limb, and therefore do not benefit from the feedback.

One way of assisting the patient in recovering lost functionality is to apply functional electrical stimulation, through patches, applied to the muscles(s) involved, where there are known relationships that determine the response of the muscles(s) to the applied stimulation, and if carefully controlled, beneficial movement results. In the first research, the reaching out task, a 2D plane movement, the patents hand was connected to a robot, and an optically based target trajectory was beamed down onto the surface. The patient then attempted to follow a moving spot over the trial length. Once complete, the error between the reference trajectory and the achieved result is available and used to compute the change in the stimulation applied on the next attempt.

In this first work, the stimulation applied to the muscle generates a torque about the elbow, which assists the patient in steering the robot as close as possible to the reference trajectory. The output is in the form of a measured angle. The ILC law is used between trials to compute the stimulation to be applied in the subsequent trial. This work was followed through to clinical trials and the research reported in the control and rehabilitation sciences literature. The clinical trials replicated the desired feature that if the patient improved with each attempt, the voluntary effort increased, and the stimulation level went down. A comprehensive treatment of this research is given in (Freeman et al., 2012; Meadmore et al., 2012).

Two desirable extensions of this first ILC healthcare research provide one source of motivation for the new results in this paper. In this application area, in the first research the trajectory (determined by healthcare professionals based on an assessment of the patients current ability) specified the reference trajectory at all instances along a trial. A more physically relevant option is to provide 'waypoints' along the trajectory or specify the starting and end locations, see, e.g. (Freeman et al., 2012). Among others, this option recognizes that no two or more people complete a task in exactly the same way. In this context, point-to-point ILC, see, e.g., (Freeman et al., 2011; Son et al., 2013) is more relevant. The task description of point-to-point ILC has been extended in (Chen et al., 2019), by considering the tracking time instants of desired positions as changing variables. Moreover, a particular case of point-to-point ILC, known as terminal ILC, has recently seen an application with supporting experimental results in agriculture (Johansen et al., 2021).

For robotic-assisted stroke rehabilitation, the eventual goal would be for patients to take equipment to their homes to increase the level of practice and avoid adding to the healthcare burden by going to a treatment center. In this sense, remote supervision would be very beneficial, but it requires reliable networked information transfer. This application provides further motivation for basic research into ILC with quantized inputs. In the point-to-point ILC design framework, much of the literature assumes that the input signal can be transmitted directly from the controller to the actuator,

and the output signal can also be transmitted directly to the controller.

In networked control systems, the system and the controller are usually physically located at different sites and communicate with each other through wired/wireless networks. Due to the limited transmission bandwidth, see, e.g., (Liu et al., 2020), the assumption that signals are transmitted accurately may no longer be valid. In some cases, it is feasible to quantify signals before transmission. Signal quantization converts continuous-valued inputs into discrete-valued inputs, which can reduce the burden of communication and improve the system's efficiency. Therefore, the effect of signal quantization on control performance needs to be addressed for point-to-point ILC laws.

Previously reported research has addressed the analysis and design of ILC with the quantized signals. For example, in (Bu et al., 2015), a logarithmic quantizer is used to quantize the output signals. Zero-error tracking performance was investigated in (Shen and Xu, 2016) for quantized error signals for discrete dynamics. This work established that the tracking error converges to a specified range with an upper bound depending on quantization density and the desired output measurement. Still, this design is not directly applicable to input quantization.

In subsequent research, an encoding-decoding mechanism was introduced to quantify the measurement output in (Huo and Shen, 2020; Zhang and Shen, 2018). This mechanism was extended in (Huo and Shen, 2020) to provide a framework for quantized ILC for systems with quantization at both the measurement and actuator sides, where zero-error tracking performance was guaranteed via an encoding-decoding mechanism. However, previous research for discrete systems has focused on the case where the reference trajectory is specified at each sample instant along the trial. The focus of this paper is the point-to-point ILC tracking problem.

As in standard control, there are simple structure ILC laws that do not necessarily require a model of the system for design. It is essential, therefore, to demonstrate that a model-based design has the potential to deliver better performance. In this paper, norm optimal ILC is considered, i.e., the control signal is designed by minimizing a cost function using a model of the dynamics. Moreover, a comparison is made with P-type ILC, i.e., $u_{k+1} = u_k + Le_k$, where a single parameter L is to be chosen.

The fault-tolerance problem for actuator faults in quantized ILC is also an important issue from the perspectives of safety and performance, especially given the updating structure. Therefore, the ILC design in this paper considers the fault-tolerant performance of actuator faults. For example, a fault-tolerant ILC scheme with quantization is given in (Gao et al., 2017), which uses the lifted model-based ILC design. An ILC algorithm is given in (Jin, 2018a) to deal with the effects of quantized input signal under actuator faults and system output constraints. The design in this paper is also extended to fault tolerance in the presence of actuator faults.

The new contributions in this paper are ILC update laws for two different quantized schemes and the novel features of these are:

- Using an encoding-decoding mechanism and the logarithmic quantizer to develop a method of quantifying the input and ILC design with a norm-optimal setting to design the ILC laws to achieve point-to-point tracking.
- The designed quantization ILC laws have passive fault-tolerance characteristics. When an actuator fault occurs, they will ensure the tracking of the desired points as the trial number increases.

The remainder of this paper is organized as follows. Section 2 describes point-to-

3

point tracking problems in linear discrete-time systems and two different quantized schemes. In Section 3, two point-to-point ILC laws are derived, and their convergence properties are established. The fault-tolerant performance of the control update laws is studied in Section 4. A numerical case study is given to demonstrate the application of new results of Section 5, and Section 6 concludes this work.

2. Problem formulation and background results

This section first introduces the system dynamics and then designs an encoding-decoding scheme for quantifying the input signals.

2.1. System dynamics

This paper considers single-input single-output discrete linear time-invariant systems described in the ILC setting by the state-space model

$$\begin{cases} x_k(t+1) = Ax_k(t) + Bu_k(t), \\ \quad y_k(t) = Cx_k(t), \end{cases} \tag{1}$$

where $x_k(t) \in \mathbb{R}^n$, $u_k(t) \in \mathbb{R}$ and $y_k(t) \in \mathbb{R}$ are, respectively, the state vector, input, and output, the subscript $k \in \mathbb{N}$ denotes the trial number, $t \in [0, \ N]$ is the sample number over finite time interval, with N denoting the total number of samples number along a trial. The state initial vector $x_k(0)$ is assumed, without loss of generality, to be the same on each trial, i.e, $x_k(0) = x_0$. Also no loss of generality arises from assuming that $x_0 = 0$.

For ILC analysis and design, the ILC dynamics are written in the so-called lifted form by introducing the vectors

$$\begin{aligned} u_k &= [u_k(0) \ u_k(1) \ \dots \ u_k(N-1)]^T, \\ y_k &= [y_k(1) \ y_k(2) \ \dots \ y_k(N)]^T, \end{aligned} \tag{2}$$

and hence

$$y_k = Gu_k, \tag{3}$$

where

$$G = \begin{bmatrix} CB & 0 & \cdots & 0 \\ CAB & CB & \cdots & 0 \\ \vdots & \vdots & \vdots & \vdots \\ CA^{N-1}B & CA^{N-2}B & \cdots & CB \end{bmatrix}. \tag{4}$$

Without loss of generality, it is assumed that $CB \neq 0$ (if this is not the case then some routine modifications are needed, see, e.g., (Owens, 2016)). The results developed in this paper generalize directly to multiple-input multiple-output examples and hence the details are omitted.

In ILC a reference trajectory y_d is specified and the design problem is to construct a sequence of trial inputs $\{u_k\}_{k \geq 0}$ such that the sequence of outputs $\{y_k\}_{k \geq 0}$ converges to

y_d as $k \to \infty$, and the input sequence to the so-called 'learned' control u_∞. Convergence is measured in terms of the norm on the underlying function space, and in applications convergence to zero error may have to be replaced by convergence to a prescribed tolerance.

Applications have also arisen where it is not necessary to enforce tracking at all instants along a trial. Instead a series of 'waypoints' along each trial are specified, known as point-to-point trajectory, or to only specify the value at the final instant N. A particularly relevant case is stroke rehabilitation where it is not necessarily required to specify desired behavior at all instants, e.g., reaching out across a table top to an object. Instead, the start and end positions can be specified and possibly one or more waypoints in between if deemed necessary based on the patients current capabilities.

Point-to-point ILC only considers the tracking performance at certain instances along the output trajectory. Let M denote the number of sample instances over $[1, \ N]$ and let t_i, $i = 1, \ldots, M$, in ascending order, denote the sample instances of interest, i.e.,

$$0 \le t_1 < t_2 < \cdots < t_M \le N. \tag{5}$$

Also y_d^p represents the point-to-point reference trajectory and introduce the lifted representation

$$y_d^p = [y_d(t_1) \ y_d(t_2) \ \ldots \ y_d(t_M)]^T, \tag{6}$$

and also

$$y_k^p = [y_k(t_1) \ y_k(t_2) \ \ldots \ y_k(t_M)]^T, \tag{7}$$

$$e_k^p = [e_k(t_1) \ e_k(t_2) \ \ldots \ e_k(t_M)]^T. \tag{8}$$

Moreover, the selection matrix $\Psi \in \mathbb{R}^{M \times N}$ is defined as

$$\Psi_{ij} = \left\{ \begin{array}{l} 1, j = t_i, \\ 0, j \ne t_i. \end{array} \right. \tag{9}$$

where this matrix provides a direct method of transforming the standard ILC problem to the point-to-point version

$$y_d^p = \Psi y_d, \ y_k^p = \Psi y_k, \ e_k^p = \Psi e_k. \tag{10}$$

These relationships will be used in the analysis below. The point-to-point ILC design problem is formulated by obvious modifications to that given above.

2.2. Quantifying the input signals

In a point-to-point tracking problem, only the signal values at the corresponding points need to be transmitted at the output side, and the bandwidth is assumed to be sufficient. For this reason, only the case of quantifying the signals at the input side before transmission is considered.

The systems represented by the block diagram of Fig. 1 are considered, where communication between the controller and actuator is via a limited capacity channel. This

scenario includes cases where only quantized information is transmitted to reduce the communication burden. Therefore, two quantization methods are used. One of these quantifies signals via an encoding and decoding mechanism, and the other quantifies the input without an encoding-decoding scheme.
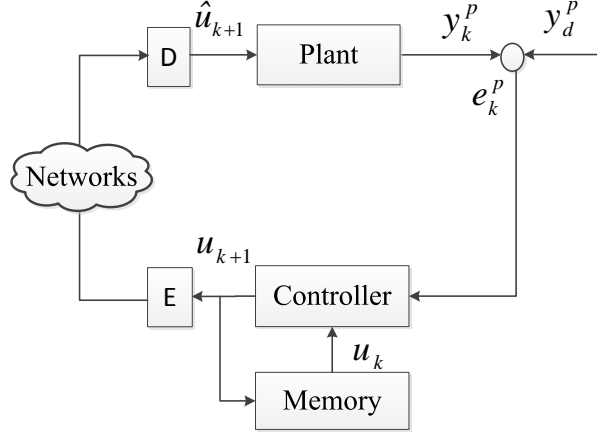
Figure 1. Block diagram of the ILC scheme considered.

The E and D blocks in Fig. 1 represent, respectively, the encoder and decoder inputs. In this structure, the controller output is first encoded by E for transmission and then decoded by D for application to the system by the actuator. The systems used are as follows:

$$E: \begin{cases} \zeta_0(t) = 0, \\ \theta_{k+1}(t) = q(u_{k+1}(t) - \zeta_k(t)), \\ \zeta_{k+1}(t) = \theta_{k+1}(t) + \zeta_k(t), \end{cases} \tag{11}$$

and

$$D: \begin{cases} \hat{u}_0(t) = 0, \\ \hat{u}_{k+1}(t) = \theta_{k+1}(t) + \hat{u}_k(t), \end{cases} \tag{12}$$

where $u_k(t)$, $\theta_k(t)$ and $\zeta_k(t)$ are, respectively, the input, output, and internal state.

The system input $\hat{u}_k(t)$ is the output of decoder D, which is an estimate of the generated input $u_k(t)$. A infinite logarithmic quantizer $q(\cdot)$ as demonstrated in (Bu et al., 2015) is used, i.e.,

$$q(v) = \begin{cases} z_i, & if \ \frac{1}{1+\delta}z_i < v \le \frac{1}{1-\delta}z_i, \\ 0, & if \ v = 0, \\ -q(-v), & if \ v < 0, \end{cases} \tag{13}$$

where $\delta = (1-\mu)/(1+\mu)$, the parameter μ is associated with the quantization density and z_i is a member of the set

$$Z = \left\{ \pm z_i | z_i = \mu^i z_0, i = 0, \pm 1, \pm 2, \cdots \right\} \bigcup \{0\}, 0 < \mu < 1, z_0 > 0. \tag{14}$$

Each of the quantization levels corresponds to a segment, i.e., the quantizer maps

6

the entire segment to this quantization level. Moreover, these segments are disjoint and their union equals the real number $\mathbb{R}$. Hence the quantizer $q(v)$ in (13) is symmetric and time-invariant.

The sector bound method given in (Fu and Xie, 2005) is used to represent the quantization error of the logarithmic quantizer. Hence, for a given quantization density μ,

$$q(v) = v + \Delta v = v + \eta \cdot v = (1 + \eta) v, \tag{15}$$

where v is the source signal of the logarithmic quantizer, Δv is the quantization error, η is the relative quantization error and $|\eta| \leq (1 - \mu)/(1 + \mu)$. Given (15), the quantizer input and output for different trials and time instants satisfy $q(v_k(t)) = (1 + \eta_k(t)) v_k(t)$.

Before designing the update law for quantifying the input with encoding-decoding scheme, it is necessary to consider the relationship between the generated input $u_k(t)$ and the system input $\hat{u}_k(t)$. Substituting $\theta_k(t)$ from the encoder into the system input $\hat{u}_k(t)$ in (11), gives

$$
\begin{aligned}
\hat{u}_{k+1}(t) &= \theta_{k+1}(t) + \hat{u}_k(t) \\
&= q(u_{k+1}(t) - \zeta_k(t)) + \hat{u}_k(t) \\
&= (1 + \eta_{k+1}(t))(u_{k+1}(t) - \zeta_k(t)) + \hat{u}_k(t) \\
&= (1 + \eta_{k+1}(t)) u_{k+1}(t) - \eta_{k+1}(t) \zeta_k(t) + \hat{u}_k(t) - \zeta_k(t),
\end{aligned} \tag{16}
$$

where $\eta_{k+1}(t)$ is the relative quantization error. Moreover, the following property for the term $\hat{u}_k(t) - \zeta_k(t)$ in (16) holds.

Proposition 1. *The term $\hat{u}_k(t) - \zeta_k(t)$ in (16) satisfies $\hat{u}_k(t) - \zeta_k(t) = 0$, $\forall\ k$.*

Proof. This proof is by mathematical induction. As the first step, $\hat{u}_0(t) = \zeta_0(t)$ due to the definitions for the encoder (11) and decoder (12), and the conclusion holds for the first step. Next, assume that the proposition holds for trial k and then the requirement is to show that it also holds for trial $k + 1$, where k is arbitrary. Using (11) and (12) gives

$$\hat{u}_{k+1}(t) - \zeta_{k+1}(t) = (\theta_{k+1}(t) + \hat{u}_k(t)) - (\theta_{k+1}(t) + \zeta_k(t)) = 0, \tag{17}$$

and by the inductive principle the proof is complete. $\square$

The inherent identity property between the encoder and decoder is used to establish the asymptotically precise data transmission and asymptotic tracking performance using quantized data. Combining Proposition 1 and (16) gives

$$\hat{u}_{k+1}(t) = (1 + \eta_{k+1}(t)) u_{k+1}(t) - \eta_{k+1}(t) \zeta_k(t). \tag{18}$$

To facilitate ILC update law design, the system input and the generated input are written in super-vector form as

$$\hat{u}_{k+1} = H_{k+1} u_{k+1} - \bar{H}_{k+1} \zeta_k, \tag{19}$$

where $H_k = diag \left(1 + \eta_k \left(0 \right) \ \ 1 + \eta_k \left(1 \right) \ \cdots \ 1 + \eta_k \left(N - 1 \right) \right)$ and $\bar{H}_k = diag \left(\eta_k \left(0 \right) \ \eta_k \left(1 \right) \ \cdots \ \eta_k \left(N - 1 \right) \right)$. Hence $H_{k+1} = \bar{H}_{k+1} + I$ and $\| H_{K+1} \| \leq 1 + \delta, \| \bar{H}_{k+1} \| \leq \delta$.

Also $q \left(u_k \left(t \right) \right) = \left(1 + \eta_k \left(t \right) \right) u_k \left(t \right)$ is used to quantize the input without encoding-decoding scheme from (15) and reformulate the logarithmic quantizer input and output as the super-vectors

$$u_k^q = q \left(u_k \right) = F_k u_k, \tag{20}$$

where $F_k = diag \left(1 + \eta_k \left(0 \right) \ \ 1 + \eta_k \left(1 \right) \ \cdots \ 1 + \eta_k \left(N - 1 \right) \right)$.

3. ILC design

The ILC design, known as norm optimal iterative learning control (NOILC), developed in this section is based on minimizing a norm-optimal cost function with the structure

$$J_{k+1} = \left\| e_{k+1}^p \right\|_Q^2 + \left\| u_{k+1} - u_k \right\|_R^2 + \left\| u_{k+1} \right\|_S^2, \tag{21}$$

where $e_{k+1}^p = y_d^p - y_{k+1}^p$ is the error on trial $k + 1$, Q and R are symmetric positive-definite weighting matrices and S is a semi-positive definite matrix, each of compatible dimensions. The induced norm on, e.g., x, is defined as $\|x\|_Q^2 = x^T Q x$. This cost function on trial $k + 1$ is the sum of a quadratic term in the current trial error, a similar term on the difference between the control signals on successive trials, and a similar term in the current trial control input.

The structure of the second term in the cost function is to regulate against large changes in the control input from one trial to the next, where in ILC it is the sequence of control inputs that are designed as opposed to the controller in other methods. Moreover, the last entry regulates the control effort.

As shown in (Zhou et al., 2022; Zhuang et al., 2022), minimizing the cost function (21) with respect to u_{k+1} gives the point-to-point ILC update law

$$u_{k+1} = T_u u_k + T_e e_k^p, \tag{22}$$

where the operators T_u and T_e are given by

$$T_u = \left[\left(\Psi G \right)^T Q \left(\Psi G \right) + R + S \right]^{-1} \left[\left(\Psi G \right)^T Q \left(\Psi G \right) + R \right],$$
$$T_e = \left[\left(\Psi G \right)^T Q \left(\Psi G \right) + R + S \right]^{-1} \left(\Psi G \right)^T Q.$$

3.1. Quantifying the input with encoding-decoding scheme

To account for the quantization error caused by quantifying the input, the cost function (21) must be modified. The relative quantization error for the logarithmic quantization is bounded by the quantization density. In quantifying the input with encoding-decoding scheme, the NOILC cost function is

$$J_{k+1} = \left\| e_{k+1}^p \right\|_Q^2 + \left\| \hat{u}_{k+1} - \hat{u}_k \right\|_R^2 + \left\| \hat{u}_{k+1} \right\|_S^2, \tag{23}$$

where $e_{k+1}^p = y_d^p - \Psi G \hat{u}_{k+1}$. $\hat{u}_k$ is not directly available on the controller side, but can be obtained indirectly by Proposition 1, i.e., $\hat{u}_k = \zeta_k$, $\forall k$. To derive the point-to-point ILC update law, the following result is needed.

Proposition 2. *Denoting the optimal solution by u_{k+1}^*, and minimizing the cost function (23) with respect to u_{k+1} gives*

$$
\begin{aligned}
u_{k+1}^* = \hat{u}_k &- H_{k+1}^{-1} \left[(\Psi G)^T Q (\Psi G) + R + S \right]^{-1} S \hat{u}_k \\
&+ H_{k+1}^{-1} \left[(\Psi G)^T Q (\Psi G) + R + S \right]^{-1} (\Psi G)^T Q e_k^p.
\end{aligned} \tag{24}
$$

Proof 1. *From (23), it follows that*

$$e_{k+1}^p = e_k^p + \Psi G \hat{u}_k - \Psi G H_{k+1} u_{k+1} + \Psi G \bar{H}_{k+1} \zeta_k = e_k^p + \Psi G H_{k+1} \hat{u}_k - \Psi G H_{k+1} u_{k+1}. \tag{25}$$

Minimizing the cost function (23) with respect to u_{k+1} gives

$$
\begin{aligned}
0 = &-H_{k+1}^T (\Psi G)^T Q \left(e_k^p + \Psi G H_{k+1} \hat{u}_k - \Psi G H_{k+1} u_{k+1}^* \right) \\
&+ H_{k+1}^T R \left(H_{k+1} u_{k+1}^* - H_{k+1} \hat{u}_k \right) + H_{k+1}^T S \left(H_{k+1} u_{k+1}^* - \bar{H}_{k+1} \hat{u}_k \right),
\end{aligned} \tag{26}
$$

and by $H_{k+1}^T = H_{k+1}$,

$$
\begin{aligned}
H_{k+1} &\left[(\Psi G)^T Q (\Psi G) + R + S \right] H_{k+1} u_{k+1}^* \\
&= H_{k+1} \left[(\Psi G)^T Q (\Psi G) + R + S \right] H_{k+1} \hat{u}_k - H_{k+1} S \hat{u}_k + H_{k+1} (\Psi G)^T Q e_k^p.
\end{aligned} \tag{27}
$$

Since H_{k+1} and $(\Psi G)^T Q (\Psi G) + R + S$ are invertible matrices, it follows that

$$
\begin{aligned}
u_{k+1}^* = \hat{u}_k &- H_{k+1}^{-1} \left[(\Psi G)^T Q (\Psi G) + R + S \right]^{-1} S \hat{u}_k \\
&+ H_{k+1}^{-1} \left[(\Psi G)^T Q (\Psi G) + R + S \right]^{-1} (\Psi G)^T Q e_k^p,
\end{aligned} \tag{28}
$$

which completes the proof.

The optimal solution in Proposition 2 contains H_{k+1}, which is not available on the current trial. To obtain an implementable ILC law and simplify the design, each non-zero element in the diagonal matrix H_{k+1} satisfies $1 - \delta \leq 1 + \eta_{k+1}(t) \leq 1 + \delta$ and hence I can be substituted for H_{k+1} to obtain an approximate optimal solution. It can be proved that the output of system can still track the desired points as the number of trials increases under this change. Hence the point-to-point ILC update law for quantifying the input with encoding-decoding scheme is

$$u_{k+1} = K_u \hat{u}_k + K_e e_k^p, \tag{29}$$

where

$$K_u = \left[(\Psi G)^T Q (\Psi G) + R + S \right]^{-1} \left[(\Psi G)^T Q (\Psi G) + R \right],$$
$$K_e = \left[(\Psi G)^T Q (\Psi G) + R + S \right]^{-1} (\Psi G)^T Q.$$

This point-to-point ILC update law modifies the input signal u_{k+1} to reduce the tracking error e_{k+1}^p gradually such that the associated output y_k^p tracks the points in y_d^p over the time horizon $[1, \ N]$. The corresponding properties are summarized in Theorem 1 given next.

Theorem 3.1. *Consider a discrete linear system of the form (3) with the encoding-decoding mechanism and the ILC update law (29) applied and let $(\Psi G)^\dagger$ denote the pseudo-inverse of (ΨG). Then if*

$$\left\| (\Psi G) (K_u - K_e \Psi G) (\Psi G)^\dagger \right\| + \delta \left\| \Psi G \right\| \left\| (K_u - K_e \Psi G - I) (\Psi G)^\dagger \right\| \le \rho_1 < 1, \quad (30)$$

the point-to-point tracking error is norm bounded in the sense that

$$\lim_{k \to \infty} \left\| e_k^p \right\| \le \frac{b_1}{1 - \rho_1}, \tag{31}$$

where $b_1 = (1 + \delta) \left\| \Psi G \right\| \left\| I - K_u \right\| \left\| u_d \right\|$.

Proof 2. *For the system (4) with the encoding-decoding mechanism, there exists a unique input u_d such that $y_d = G u_d$. Set $\Delta u_k \overset{\Delta}{=} u_d - \hat{u}_k$ and it then follows from (19) that*

$$\Delta u_{k+1} = u_d - \hat{u}_{k+1} = u_d - \left(H_{k+1} u_{k+1} - \bar{H}_{k+1} \zeta_k \right). \tag{32}$$

By Proposition 1, $\hat{u}_k(t) = \zeta_k(t), \ \forall \ k$, and substituting (29) into this last equation gives

$$\Delta u_{k+1} = u_d - \hat{u}_{k+1} = u_d - H_{k+1} \left(K_u \hat{u}_k + K_e e_k^p \right) + \bar{H}_{k+1} \hat{u}_k, \tag{33}$$

and from (10)

$$e_k^p = y_d^p - y_k^p = \Psi G u_d - \Psi G \hat{u}_k = \Psi G \Delta u_k. \tag{34}$$

Substituting (34) and $\hat{u}_k = u_d - \Delta u_k$ into (33) gives

$$\begin{aligned} \Delta u_{k+1} &= u_d - H_{k+1} K_u (u_d - \Delta u_k) - H_{k+1} K_e \Psi G \Delta u_k + \bar{H}_{k+1} (u_d - \Delta u_k) \\ &= \left(I - H_{k+1} K_u + \bar{H}_{k+1} \right) u_d + \left(H_{k+1} K_u - H_{k+1} K_e \Psi G - \bar{H}_{k+1} \right) \Delta u_k. \end{aligned} \tag{35}$$

Given $e_k^p = \Psi G \Delta u_k$, it follows that

$$e_{k+1}^p = \Psi G \left(I - H_{k+1} K_u + \bar{H}_{k+1} \right) u_d + \Psi G \left(H_{k+1} K_u - H_{k+1} K_e \Psi G - \bar{H}_{k+1} \right) (\Psi G)^\dagger e_k^p. \tag{36}$$

10

and taking the norm across this last equation gives

$$\left\|e_{k+1}^p\right\| \leq \left\|\Psi G\left(I - H_{k+1}K_u + \bar{H}_{k+1}\right)\right\| \|u_d\| \\ + \left\|\Psi G\left(H_{k+1}K_u - H_{k+1}K_e\Psi G - \bar{H}_{k+1}\right)(\Psi G)^\dagger\right\| \|e_k^p\|. \tag{37}$$

If $\left\|(\Psi G)(K_u - K_e\Psi G)(\Psi G)^\dagger\right\| + \delta\|\Psi G\|\left\|(K_u - K_e\Psi G - I)(\Psi G)^\dagger\right\| \leq \rho_1 < 1$ *holds, then*

$$\begin{aligned} &\left\|\Psi G\left(H_{k+1}K_u - H_{k+1}K_e\Psi G - \bar{H}_{k+1}\right)(\Psi G)^\dagger\right\| \\ &= \left\|\Psi G\left[(K_u - K_e\Psi G) + \bar{H}_{k+1}(K_u - K_e\Psi G - I)\right](\Psi G)^\dagger\right\| \\ &\leq \left\|\Psi G(K_u - K_e\Psi G)(\Psi G)^\dagger\right\| + \|\Psi G\|\left\|\bar{H}_{k+1}\right\|\left\|(K_u - K_e\Psi G - I)(\Psi G)^\dagger\right\| \\ &\leq \left\|\Psi G(K_u - K_e\Psi G)(\Psi G)^\dagger\right\| + \delta\|\Psi G\|\left\|(K_u - K_e\Psi G - I)(\Psi G)^\dagger\right\| \\ &\leq \rho_1 < 1. \end{aligned} \tag{38}$$

Next, define

$$\left\|\Psi G\left(I - H_{k+1}K_u + \bar{H}_{k+1}\right)\right\| \|u_d\| = \left\|\Psi G\left(H_{k+1} - H_{k+1}K_u\right)\right\| \|u_d\| \\ = \|\Psi G H_{k+1}(I - K_u)\| \|u_d\| \leq (1 + \delta)\|\Psi G\|\|I - K_u\|\|u_d\| = b_1, \tag{39}$$

and then combined with (37), (38) and (39), we have

$$\left\|e_{k+1}^p\right\| \leq b_1 + \rho_1\left\|e_k^p\right\|. \tag{40}$$

After k executions of the last formula, the following inequality is established

$$\left\|e_{k+1}^p\right\| \leq \frac{1 - \rho_1^{k+1}}{1 - \rho_1}b_1 + \rho_1^k\left\|e_0^p\right\|. \tag{41}$$

Applying $\lim\limits_{k\to\infty} \rho_1^k = 0$ *to this last inequality gives*

$$\lim_{k\to\infty}\left\|e_k^p\right\| \leq \frac{b_1}{1 - \rho_1}, \tag{42}$$

and the proof is complete.

From the proof of Theorem 1, if the last term $\|\hat{u}_{k+1}\|_S^2$ is deleted from the cost function, the point-to-point tracking error e_k^p also converges as $k \to \infty$ to zero, which is established by the following corollary to the last theorem.

Corollary 1. *If* $S = 0$, *and*

$$\left\|(\Psi G)(K_u - K_e\Psi G)(\Psi G)^\dagger\right\| + \delta\|\Psi G\|\left\|(K_u - K_e\Psi G - I)(\Psi G)^\dagger\right\| \leq \rho_1 < 1$$

the point-to-point tracking error converges to zero as $k \to \infty$, *i.e.,* $\lim\limits_{k\to\infty}\left\|e_k^p\right\| = 0$.

11

Proof 3. *When $S = 0$*

$$I - K_u = I - \left[(\Psi G)^T Q (\Psi G) + R \right]^{-1} \left[(\Psi G)^T Q (\Psi G) + R \right] = 0. \qquad (43)$$

Moreover

$$\left\| \Psi G \left(I - H_{k+1} K_u + \bar{H}_{k+1} \right) \right\| \|u_d\| \le \delta \|\Psi G\| \|I - K_u\| \|u_d\| = b_1 = 0, \qquad (44)$$

and by combining with the result of Theorem 1

$$0 \le \lim_{k \to \infty} \left\| e_k^p \right\| \le \frac{b_1}{1 - \rho_1} = 0, \qquad (45)$$

which completes the proof.

Remark 1. If $S \ne 0$

$$b_1 = (1 + \delta) \|\Psi G\| \left\| \left[(\Psi G)^T Q (\Psi G) + R + S \right]^{-1} S \right\| \|u_d\|, \qquad (46)$$

i.e., when different quantization densities are used, the tracking error converges in norm to a bounded value by appropriate choice of the cost function weighting matrices Q, R and S.

3.2. Quantifying the input without encoding-decoding scheme

As for quantifying input signals without encoding-decoding scheme, the cost function used is

$$J_{k+1} = \left\| e_{k+1}^p \right\|_Q^2 + \left\| u_{k+1}^q - u_k^q \right\|_R^2 + \left\| u_{k+1}^q \right\|_S^2, \qquad (47)$$

where $e_{k+1}^p = y_d^p - \Psi G u_{k+1}^q = e_k^p + \Psi G u_k^q - \Psi G F_{k+1} u_{k+1}$. Minimizing this function with respect to u_{k+1} gives

$$\begin{aligned} u_{k+1}^* = &F_{k+1}^{-1} \left[(\Psi G)^T Q (\Psi G) + R + S \right]^{-1} \left[(\Psi G)^T Q (\Psi G) + R \right] u_k^q \\ &+ F_{k+1}^{-1} \left[(\Psi G)^T Q (\Psi G) + R + S \right]^{-1} (\Psi G)^T Q e_k^p, \end{aligned} \qquad (48)$$

where u_{k+1}^* denoted the optimal solution for the cost function (47). Similar to the previous section, substitute I for F_{k+1} to obtain the approximate optimal solution, and then the implementable ILC law can be written as

$$u_{k+1} = L_u u_k^q + L_e e_k^p, \qquad (49)$$

where

$$L_u = \left[(\Psi G)^T Q (\Psi G) + R + S \right]^{-1} \left[(\Psi G)^T Q (\Psi G) + R \right],$$
$$L_e = \left[(\Psi G)^T Q (\Psi G) + R + S \right]^{-1} (\Psi G)^T Q.$$

Then, the following result gives the stability property of this ILC law.

Theorem 3.2. *Consider a linear discrete-time system (3) where the input signals are quantized without encoding-decoding scheme and the ILC law (49) is applied. Then if*

$$\left\| (\Psi G) (L_u - L_e \Psi G) (\Psi G)^\dagger \right\| + \delta \|\Psi G\| \left\| (L_u - L_e \Psi G) (\Psi G)^\dagger \right\| \le \rho_2 < 1, \qquad (50)$$

and the point-to-point tracking error satisfies

$$\lim_{k \to \infty} \left\| e_k^p \right\| \le \frac{b_2}{1 - \rho_2}, \qquad (51)$$

where $b_2 = (\|\Psi G (I - L_u)\| + \delta \|\Psi G\| \|L_u\|) \|u_d\|$.

Proof 4. *Set* $\Delta u_k := u_d - u_k^q$ *and following similar steps as in the proof of Theorem 1 gives*

$$
\begin{aligned}
\left\| e_{k+1}^p \right\| &\le \|\Psi G (I - F_{k+1} L_u)\| \|u_d\| + \left\| \Psi G F_{k+1} (L_u - L_e \Psi G) (\Psi G)^\dagger \right\| \left\| e_k^p \right\| \\
&\le \left(\left\| \Psi G (L_u - L_e \Psi G) (\Psi G)^\dagger \right\| + \delta \|\Psi G\| \left\| (L_u - L_e \Psi G) (\Psi G)^\dagger \right\| \right) \left\| e_k^p \right\| \\
&\quad + (\|\Psi G (I - L_u)\| + \delta \|\Psi G\| \|L_u\|) \|u_d\|.
\end{aligned}
\qquad (52)
$$

Also, if $\left\| (\Psi G) (L_u - L_e \Psi G) (\Psi G)^\dagger \right\| + \delta \|\Psi G\| \left\| (L_u - L_e \Psi G) (\Psi G)^\dagger \right\| \le \rho_2 < 1$, *it follows that*

$$\lim_{k \to \infty} \left\| e_k^p \right\| \le \frac{b_2}{1 - \rho_2}, \qquad (53)$$

where $(\|\Psi G (I - L_u)\| + \delta \|\Psi G\| \|L_u\|) \|u_d\| = b_2$. *This completes the proof.*

Remark 2. By $\delta = \frac{1-\mu}{1+\mu}$, a larger quantization density μ results in a smaller relative quantization error and $|\eta| \le \delta$. Also $L_u = I$ when $S = 0$ and hence

$$\|\Psi G (I - F_{k+1} L_u)\| \|u_d\| = \left\| \Psi G \bar{F}_{k+1} \right\| \|u_d\| \le \delta \|\Psi G\| \|u_d\| = b_2.$$

In contrast to the encoding and decoding scheme considered above, the tracking error converges in the norm to a bounded value that depends on the quantization density in quantifying the input without encoding-decoding scheme.

Remark 3. The basic idea of quantization is to actively reduce information content for adapting to the limitation of transmission channel bandwidth. For the logarithmic

quantizer, when the quantization density is closer to the unit, the information transmitted is more accurate, but the equipment and channel bandwidth requirements are higher. The smaller the quantization density is, the more information is lost, which leads to a greater quantization error.

The inherent property of the logarithmic quantizer is that a smaller source signal results in a smaller quantization error. The encoding and decoding schemes essentially quantify the change of input between the previous and current trial. When the sequence whose entries are the changes between the control input on two successive trials converges as the number of trials increases, the quantization error also reduces. Consequently, the encoding and decoding scheme can perform well even if the quantizer is coarse. However, the quantization density must have the largest possible value within the bandwidth to result in better tracking performance for quantifying the input without encoding-decoding scheme

4. ILC Fault-tolerant performance

Actuator faults are as critical in ILC as in other areas, which may cause unsatisfactory performance or even instability. In such cases, it is necessary to design the update law such that the system output can ensure tracking in the presence of actuator failures. For the control input $\hat{u}_k(t)$ from quantifying the input with the encoding-decoding scheme, let $u_k^F(t)$ denote the signal from the failed actuator, where the superscript F denotes the presence of a fault. Then (Wang et al., 2012), the following failure model can be considered

$$u_k^F(t) = \alpha_i \hat{u}_k(t), i = 0, 1, \cdots, N-1, \tag{54}$$

where α_i is the fault parameter, and $0 \le \underline{\alpha_i} \le \alpha_i \le 1$, $i = 0, 1, \cdots, N-1$, and $\underline{\alpha_i}$ is a known scalar.

The parameter α_i is unknown but assumed to lie within a known range. If $\alpha_i = 1$, the actuator is fault-free. Also, $0 < \alpha_i < 1$ corresponds to a partial failure due to, e.g., mechanical wear and aging. If $\alpha_i = 0$, then the actuator has a complete failure, and the system is no longer controllable. In this paper, only $0 < \alpha_i \le 1$ is considered.

Introduce

$$\begin{aligned} u_k^F &= \begin{bmatrix} u_k^F(0) & u_k^F(1) & \cdots & u_k^F(N-1) \end{bmatrix}^T, \\ \hat{u}_k &= \begin{bmatrix} \hat{u}_k(0) & \hat{u}_k(1) & \cdots & \hat{u}_k(N-1) \end{bmatrix}^T, \\ \alpha &= diag\left(\alpha_0 \ \alpha_1 \ \cdots \ \alpha_{N-1}\right). \end{aligned}$$

Then the failure model can be written as

$$u_k^F = \alpha \hat{u}_k, \tag{55}$$

and hence

$$y_k^p = \Psi G u_k^F = \Psi G \alpha \hat{u}_k. \tag{56}$$

The following assumption is also required.

Assumption 1. *There exists a desired input u_d such that $u_d^F = \alpha u_d$ satisfies $y_d^p = \Psi G u_d^F$.*

Remark 4. To clarify the rationality of the statement in Assumption 1, let $(\Psi G)^\dagger$ denote the pseudo-inverse of (ΨG). Then. from $y_d^p = \Psi G u_d^F$, it follows that

$$u_d^F = (\Psi G)^\dagger y_d^p, \tag{57}$$

and from the failure model, it follows that

$$u_d^F = \alpha \hat{u}_d, \tag{58}$$

where $\hat{u}_d = u_d$ and

$$\alpha = \begin{bmatrix} \alpha_0 & \cdots & 0 \\ \vdots & \ddots & \vdots \\ 0 & \cdots & \alpha_{N-1} \end{bmatrix}, \ 0 < \alpha_i \leq 1. \tag{59}$$

Consequently, there exists a desired input u_d that satisfies

$$u_d = \alpha^{-1} u_d^F = \alpha^{-1} (\Psi G)^\dagger y_d^p. \tag{60}$$

To proceed, introduce

$$\Delta \alpha = diag \left(\Delta \alpha_0 \ \Delta \alpha_1 \cdots \Delta \alpha_{N-1} \right), \tag{61}$$

such that $\alpha = I + \Delta \alpha$. Then the fault-tolerant property for quantifying the input with encoding-decoding scheme can be established.

Theorem 4.1. *Consider a linear discrete-time system described by(3) with encoding-decoding mechanism and ILC update law (29) applied. Then if*

$$
\begin{aligned}
&\left\| \Psi G \left(I - K_e \Psi G \right) (\Psi G)^\dagger \right\| + \delta \left\| \Psi G \right\| \left\| K_e \right\| + (1 + \delta) \left\| \Psi G \right\| \left\| \Delta \alpha \right\| \left\| K_e \right\| \\
&+ (1 + \delta) \frac{1 + \|\Delta\alpha\|}{1 - \|\Delta\alpha\|} \left\| \Psi G \right\| \left\| K_u - I \right\| \left\| (\Psi G)^\dagger \right\| \leq \rho_3 < 1,
\end{aligned} \tag{62}
$$

the system has the actuator fault-tolerant capability, and the point-to-point tracking error satisfies

$$\lim_{k \to \infty} \left\| e_k^p \right\| = \frac{b_3}{1 - \rho_3}, \tag{63}$$

where $(1 + \delta) (1 + \|\Delta\alpha\|) \|\Psi G\| \|I - K_u\| \|u_d\| = b_3$.

Proof 5. *Set $\Delta u_k := u_d - \hat{u}_k$, and then from (19) it follows that*

$$\Delta u_{k+1} = u_d - \hat{u}_{k+1} = u_d - H_{k+1} u_{k+1} + \bar{H}_{k+1} \hat{u}_k. \tag{64}$$

Substituting (29) into the last equation gives

$$\Delta u_{k+1} = u_d - \hat{u}_{k+1} = u_d - H_{k+1}\left(K_u\hat{u}_k + K_e e_k^p\right) + \bar{H}_{k+1}\hat{u}_k, \tag{65}$$

and using (10) it follows that

$$e_k^p = y_d^p - y_k^p = \Psi G u_d^F - \Psi G \hat{u}_k^F = \Psi G\alpha u_d - \Psi G\alpha\hat{u}_k = \Psi G\alpha\Delta u_k. \tag{66}$$

Substituting (66) and $\hat{u}_k = u_d - \Delta u_k$ into (65) gives

$$\begin{aligned}\Delta u_{k+1} &= u_d - H_{k+1}K_u\left(u_d - \Delta u_k\right) - H_{k+1}K_e\Psi G\alpha\Delta u_k + \bar{H}_{k+1}\left(u_d - \Delta u_k\right) \\ &= \left(I - H_{k+1}K_u + \bar{H}_{k+1}\right)u_d + \left(H_{k+1}K_u - H_{k+1}K_e\Psi G\alpha - \bar{H}_{k+1}\right)\Delta u_k.\end{aligned} \tag{67}$$

Since $e_{k+1}^p = \Psi G\alpha\Delta u_{k+1}$, it follows that

$$\begin{aligned}e_{k+1}^p =\ &\Psi G\alpha\left(I - H_{k+1}K_u + \bar{H}_{k+1}\right)u_d \\ &+ \Psi G\alpha\left(H_{k+1}K_u - H_{k+1}K_e\Psi G\alpha - \bar{H}_{k+1}\right)\alpha^{-1}\left(\Psi G\right)^{\dagger}e_k^p.\end{aligned} \tag{68}$$

Taking the norm to this last equation gives

$$\begin{aligned}\left\|e_{k+1}^p\right\| \leq\ &\left\|\Psi G\alpha\left(I - H_{k+1}K_u + \bar{H}_{k+1}\right)\right\|\left\|u_d\right\| \\ &+ \left\|\Psi G\alpha\left(H_{k+1}K_u - H_{k+1}K_e\Psi G\alpha - \bar{H}_{k+1}\right)\alpha^{-1}\left(\Psi G\right)^{\dagger}\right\|\left\|e_k^p\right\|,\end{aligned} \tag{69}$$

Also

$$\begin{aligned}\left\|\Psi G\alpha\left(I - H_{k+1}K_u + \bar{H}_{k+1}\right)\right\|\left\|u_d\right\| &\leq \left\|\Psi G\right\|\left\|I + \Delta\alpha\right\|\left\|H_{k+1}\right\|\left\|I - K_u\right\|\left\|u_d\right\| \\ &\leq (1 + \delta)\left(1 + \left\|\Delta\alpha\right\|\right)\left\|\Psi G\right\|\left\|I - K_u\right\|\left\|u_d\right\| = b_3.\end{aligned} \tag{70}$$

If the inequality (62) holds, then

$$\begin{aligned}&\left\|\Psi G\alpha\left(H_{k+1}K_u - H_{k+1}K_e\Psi G\alpha - \bar{H}_{k+1}\right)\alpha^{-1}\left(\Psi G\right)^{\dagger}\right\| \\ &= \left\|\Psi G\left(I - H_{k+1}\alpha K_e\Psi G + H_{k+1}\alpha\left(K_u - I\right)\alpha^{-1}\right)\left(\Psi G\right)^{\dagger}\right\| \\ &\leq \left\|\Psi G\left(I - H_{k+1}\alpha K_e\Psi G\right)\left(\Psi G\right)^{\dagger}\right\| + \left\|\Psi G\left(H_{k+1}\alpha\left(K_u - I\right)\alpha^{-1}\right)\left(\Psi G\right)^{\dagger}\right\| \\ &\leq \left\|\Psi G\left(I - K_e\Psi G\right)\left(\Psi G\right)^{\dagger}\right\| + \left\|\Psi G\right\|\left\|\Delta\alpha\right\|\left\|K_e\right\| + \left\|\Psi G\right\|\left\|\bar{H}_{k+1}\right\|\left\|K_e\right\| \\ &\quad + \left\|\Psi G\right\|\left\|\bar{H}_{k+1}\right\|\left\|\Delta\alpha\right\|\left\|K_e\right\| + \left\|\Psi G\right\|\left\|H_{k+1}\right\|\left\|I + \Delta\alpha\right\|\left\|K_u - I\right\|\left\|\alpha^{-1}\right\|\left\|\left(\Psi G\right)^{\dagger}\right\| \\ &\leq \left\|\Psi G\left(I - K_e\Psi G\right)\left(\Psi G\right)^{\dagger}\right\| + \delta\left\|\Psi G\right\|\left\|K_e\right\| + (1 + \delta)\left\|\Psi G\right\|\left\|\Delta\alpha\right\|\left\|K_e\right\| \\ &\quad + (1 + \delta)\frac{1 + \left\|\Delta\alpha\right\|}{1 - \left\|\Delta\alpha\right\|}\left\|\Psi G\right\|\left\|K_u - I\right\|\left\|\left(\Psi G\right)^{\dagger}\right\| \\ &\leq \rho_3 < 1.\end{aligned} \tag{71}$$

Substituting (70) and (71) into (69) gives

$$\left\|e_{k+1}^p\right\| \leq b_3 + \rho_3\left\|e_k^p\right\|. \tag{72}$$

16

After k trials it follows that

$$\left\| e_{k+1}^p \right\| \leq \frac{1 + \rho_3^{k+1}}{1 - \rho_3} b_3 + \rho_3^k \left\| e_0^p \right\|. \tag{73}$$

Also since $\lim\limits_{k \to \infty} \rho_3^k = 0$

$$\lim_{k \to \infty} \left\| e_k^p \right\| \leq \frac{b_3}{1 - \rho_3}. \tag{74}$$

This completes the proof.

Remark 5. Passive fault-tolerance is used in this paper by considering the actuator faults to design an ILC law to improve the reliability of the system. Quantifying the input with encoding-decoding scheme can guarantee the tracking performance of the networked system in the presence of faults.

Remark 6. Consider the case when $S = 0$, $K_u = I$. It follows that $b_3 = (1 + \delta)(1 + \|\Delta\alpha\|) \|\Psi G\| \|I - K_u\| \|u_d\| = 0$ and, by combining with the result of Theorem 4.1, $\lim\limits_{k \to \infty} \left\| e_k^p \right\| = 0$.

For control input $u_k^q(t)$, let $u_k^F(t)$ denote the signal from the failed actuator. Then (Wang et al., 2012), the following failure model can be used

$$u_k^F(t) = \alpha u_k^q(t), i = 0, 1, \cdots, N - 1, \tag{75}$$

or

$$u_k^F = \alpha q(u_k), \tag{76}$$

where

$$u_k^F = \left[u_k^F(0) \ u_k^F(1) \ \cdots \ u_k^F(N-1) \right]^T,$$
$$u_k^q = \left[u_k^q(0), u_k^q(1), \cdots, u_k^q(N-1) \right]^T,$$
$$\alpha = diag\left(\alpha_0 \ \alpha_1 \ \cdots \ \alpha_{N-1} \right).$$

Hence, there exists

$$y_k^p = \Psi G u_k^F = \Psi G \alpha u_k^q \tag{77}$$

and the following theorem can be established.

Theorem 4.2. *Consider the system (4) when the input signals are quantified without an encoding-decoding scheme. Suppose also the ILC law (49) is applied. Then if*

$$\left\| \Psi G (I - L_e \Psi G)(\Psi G)^\dagger \right\| + \delta \|\Psi G\| \left\| (I - L_e \Psi G)(\Psi G)^\dagger \right\| + \|\Psi G\| \|\Delta\alpha\| \|L_e\|$$
$$+ \delta \|\Psi G\| \|\Delta\alpha\| \|L_e\| + (1 + \delta) \frac{1 + \|\Delta\alpha\|}{1 - \|\Delta\alpha\|} \|\Psi G\| \|K_u - I\| \left\| (\Psi G)^\dagger \right\| \leq \rho_4 < 1, \tag{78}$$

the system has the actuator fault-tolerant capability,and the norm-bounded point-to-point tracking error satisfies

$$\lim_{k \to \infty} \left\| e_k^p \right\| \leq \frac{b_4}{1 - \rho_4}, \tag{79}$$

where $\left(\|I - L_u\| + \delta \|L_u\| \right) \left(1 + \|\Delta\alpha\| \right) \|\Psi G\| \|u_d\| = b_4$.

Proof 6. *Set* $\Delta u_k := u_d - u_k^q$ *and define* $\|\Psi G\alpha \left(I - F_{k+1} L_u \right)\| \|u_d\| \leq \|\Psi G\alpha\| \left(\|I - L_u\| + \left\| \bar{F}_{k+1} L_u \right\| \right) \|u_d\| \leq \left(\|I - L_u\| + \delta \|L_u\| \right) \left(1 + \|\Delta\alpha\| \right) \|\Psi G\| \|u_d\| = b_4$. *The proof from this stage follows by routine changes to that for Theorem 3, and hence the details are omitted for brevity.*

5. Simulation case study

In this section, the effectiveness of the new design approach developed in this paper is demonstrated using a simulation case study, which uses the model of one axis of a gantry robot testbed (Ratcliffe, 2004) that has been obtained from measured frequency response tests. Network communication is used between the system and controller with communication bandwidth capacity. Therefore, the controller output has to be quantized by a logarithmic quantizer before transmission to the actuator. The system output only needs to transmit the tracking errors at selected sample instants to the control law, and it is not necessary to quantify them.

A proportional feedback control loop with gain 300 has been applied and the transfer-function of the axis dynamics has been discretized with a sampling time of $Ts = 0.01s$ to get discrete transfer-function

$$G(z) = \frac{0.0003507z^2 + 0.00003062z + 2.164 \times 10^{-6}}{z^3 - 0.8798z^2 - 0.004291z - 0.0008451}, \tag{80}$$

whose discrete state space model matrices are shown as follows

$$A = \begin{bmatrix} 0.0214 & 0.0451 & 0.0124 \\ -0.0515 & -0.0497 & -0.1771 \\ 0.0916 & 0.1202 & 0.9081 \end{bmatrix},$$
$$B = \begin{bmatrix} -5.0269 \times 10^{-5} & 7.1601 \times 10^{-4} & 3.7143 \times 10^{-4} \end{bmatrix}^T,$$
$$C = \begin{bmatrix} 0 & 0.0621 & 0.8245 \end{bmatrix}.$$

In the state-space equations, the input variable $u_k(t)$ denotes the input voltage, and the output variable $y_k(t)$ denotes the position of z-axis of the gantry robot, and then the lifted form model $y_k = Gu_k$ can be obtained.

The reference trajectory is of the point-to-point form with $M = 5$ and associated reference trajectory

$$y_d^p = [0.0029, \ -0.0048, \ 0.0048, \ -0.0029, \ 0]^T, \tag{81}$$

with a trial length of $T = 2$ seconds and hence $N = 200$.

The five reference instances correspond to

$$t_1 = 0.2s, \ t_2 = 0.6s, \ t_3 = 1.0s, \ t_4 = 1.4s, \ t_5 = 2.0s. \tag{82}$$

Hence the performance requirement for this system to move from the initial position to $y_d(t_1)$ at the specified time t_1, and then to $y_d(t_2)$ at specified time t_2 and likewise for the other three. For the initial design studies, the weighting matrices in the cost function are taken to have the diagonal forms $Q = qI$, $R = rI$, $S = sI$, where q, r are positive scalars and s is nonnegative scalar. Also the initial input signal is taken as $u_0 = 0$.
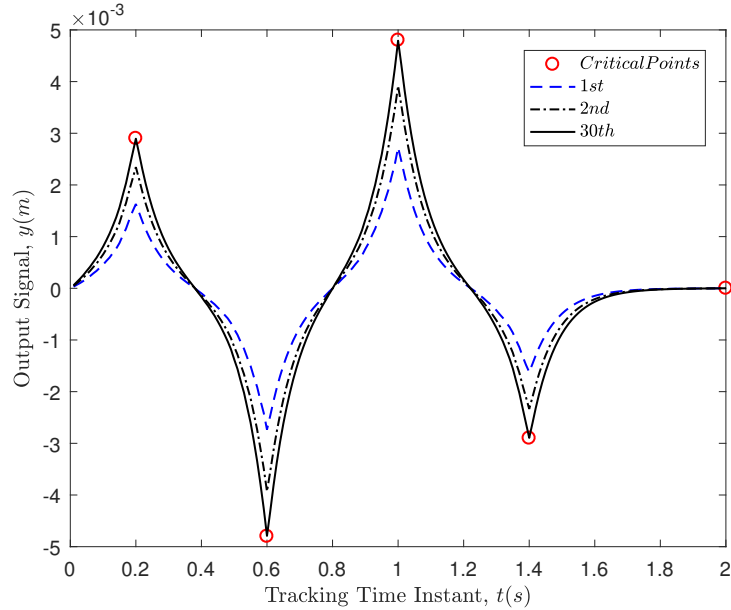
Figure 2. Output trajectories for quantifying the input with encoding-decoding scheme over the first few trials and the final trial (i.e., 30).

Consider quantifying the input with the encoding-decoding scheme, and set $z_0 = 2$ and $\mu = 0.8$ in the logarithmic quantizer. Choosing the weighting parameters as $q = 80,000$, $r = 0.04$, $s = 0.0001$, we can obtain the control law matrices K_u and K_e (not shown for ease of presentation) then (29) results in $\left\| (\Psi G)(K_u - K_e \Psi G)(\Psi G)^\dagger \right\| + \delta \left\| \Psi G \right\| \left\| (K_u - K_e \Psi G - I)(\Psi G)^\dagger \right\| = 0.4338 < 1$. Hence Theorem 1 holds in this case and consider the case that the controlled system is simulated for 30 trials. Fig. 2 confirms that trial outputs trajectories converge to the reference values (marked by the red circles in the figure). Hence quantifying the input with encoding-decoding scheme is effective for the point-to-point tracking task under limited communication bandwidth.

The corresponding input signals are shown in Fig. 3, which confirms that this signal approaches the learned control one as the trial number increases. Moreover, as a comparison with a non-model based ILC consider the P-type ILC law $u_{k+1} = u_k + L\Psi^T e_k^p$ for the particular case when $L = 1200$. Then Fig. 4 leads to the conclusion that the design in this paper has a faster convergence rate than the P-type ILC (the case
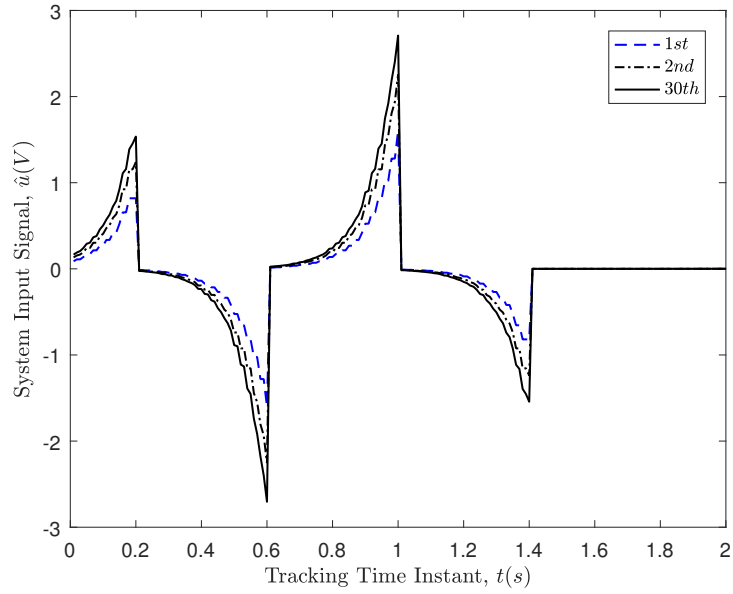
Figure 3. System input signals for quantifying the input with encoding-decoding scheme over the first few trials and the final trial (i.e., 30) .
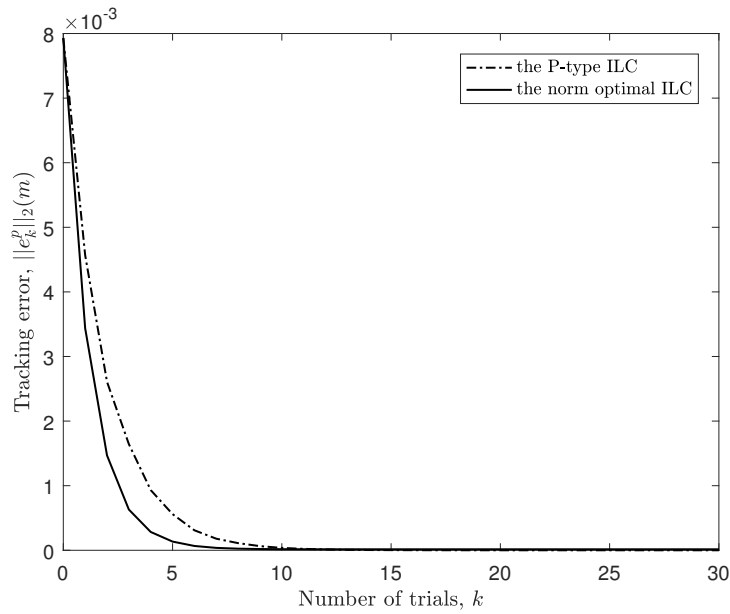

Figure 4. A comparison of tracking error between the norm optimal ILC and the P-type ILC.

considered is quantifying the input with the encoding-decoding scheme. (An area for possible future research is to investigate the performance of the new design against other non-model based ILC designs.)

To illustrate the effect of q, consider the parameters r and s to be fixed and let

20
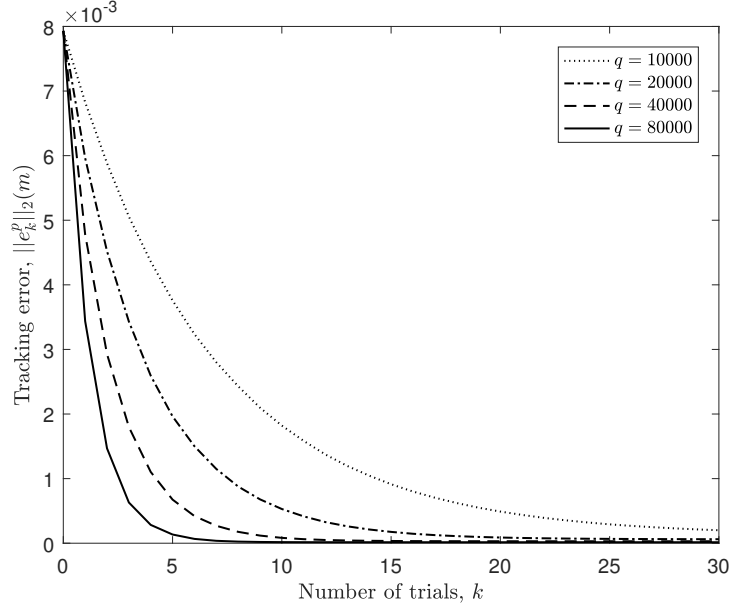
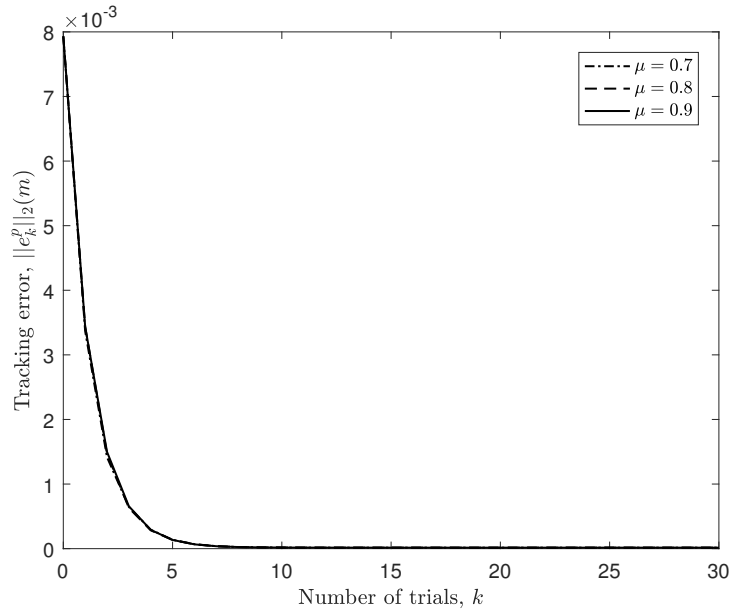**Figure 5.** Tracking error of different value q for quantifying the input with encoding-decoding scheme.
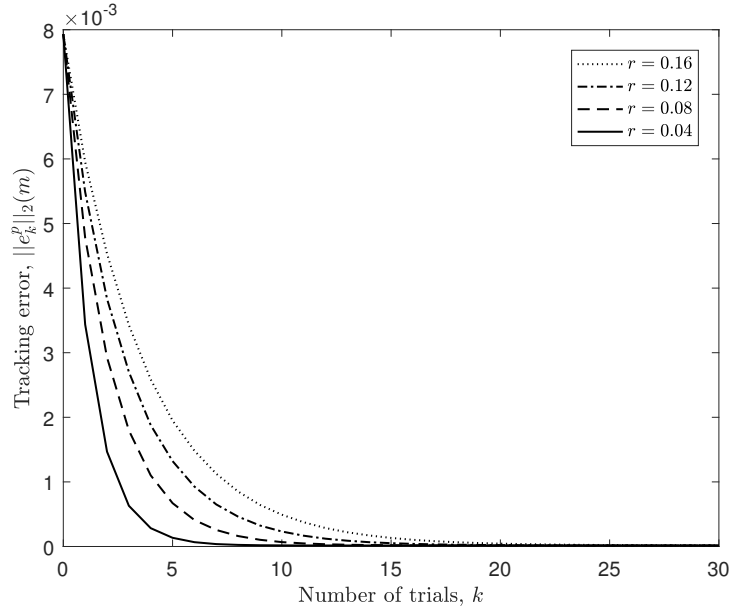
Figure 6. Tracking error of different value r for quantifying the input with encoding-decoding scheme.

q is a variable parameter. Setting $r = 0.04$ and $s = 0.0001$, simulations for different values of q have been undertaken. Over 30 trials, the resulting tracking error is shown in Fig. 5. The larger q will result in a faster rate of decrease for the tracking error and the value of parameter q relative to parameter s will affect the tracking accuracy. Similarly, the effects of r and s are shown in Fig. 6 and Fig. 7. The smaller r will

21
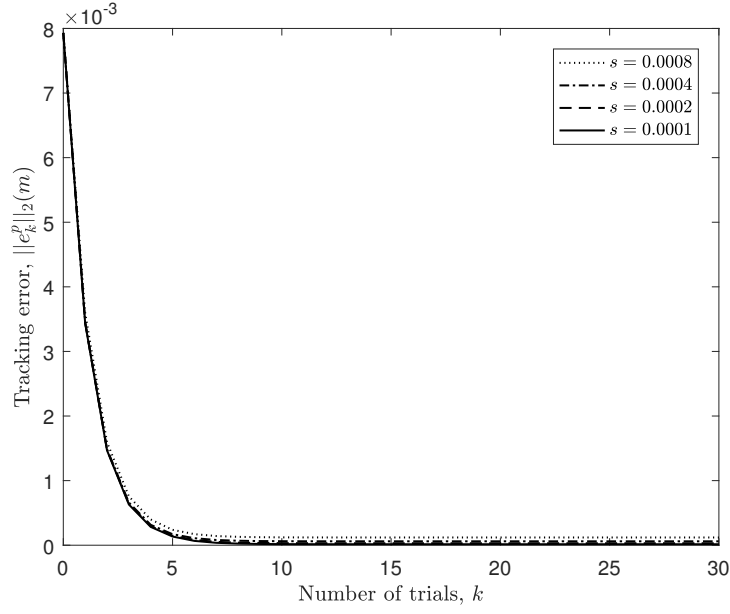
Figure 7. Tracking error of different value s over 30 ILC trials for encoding-decoding scheme.

result in a faster rate of decrease for the tracking error, but input change between the previous trial and the next trial will more obvious and the smaller s will lead to the smaller tracking error.
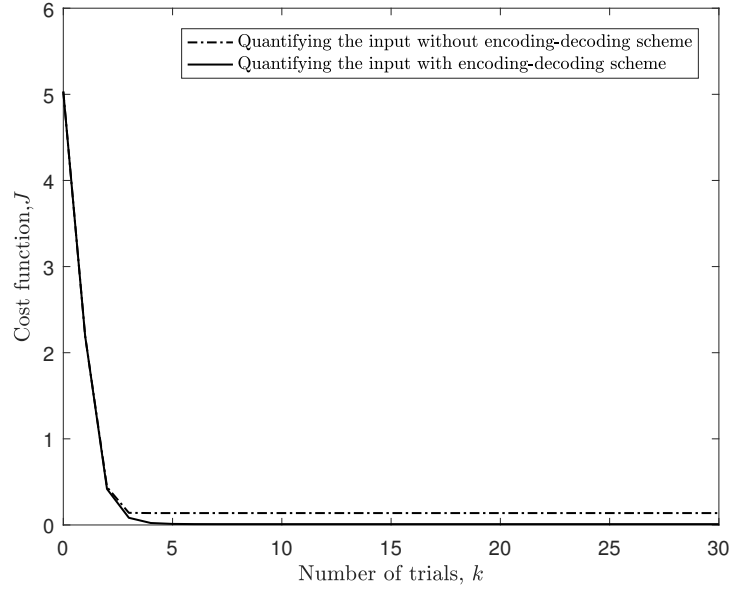

Figure 8. Tracking error of different quantization density for quantifying the input with encoding-decoding scheme.

To understand the effect of quantization, simulations with different quantization
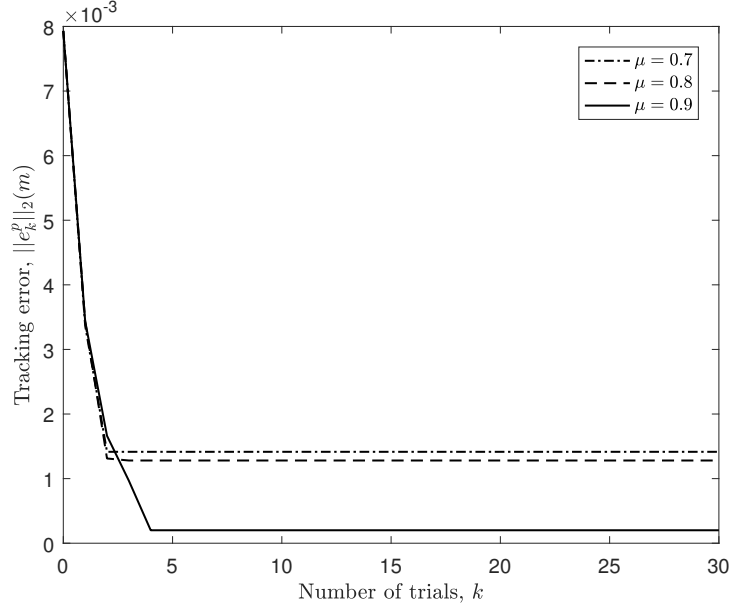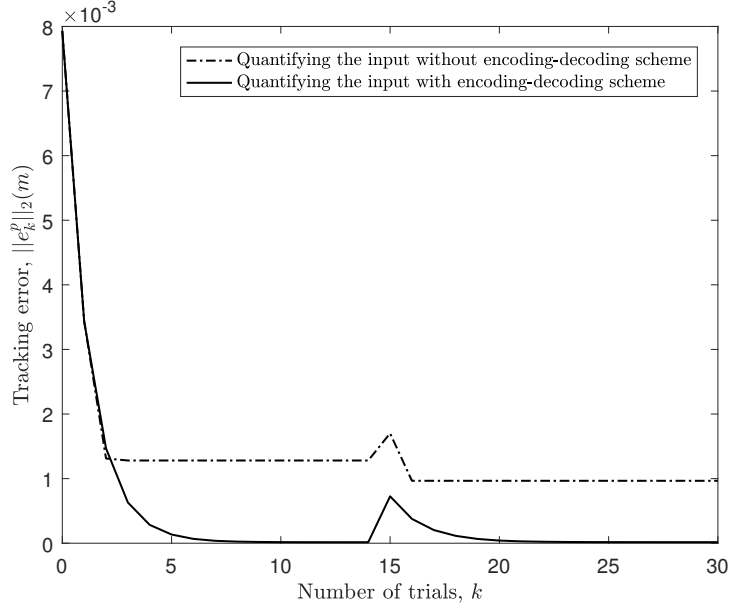
Figure 9. Tracking error of different quantization density for quantifying the input without encoding-decoding scheme.

Figure 10. Cost function comparison of different quantization scheme along the trial axis.

densities μ for the two different quantization schemes were undertaken using the same cost function weighting parameters. Over 30 trials, the resulting tracking error is shown in Fig. 8 for the first scheme and Fig. 9 for the second. It is seen that the tracking performance for quantifying the input with encoding-decoding scheme is similar under different quantization densities, and the tracking performance improves with the

Figure 11. Tracking error comparison of different quantization scheme with actuator fault.

increase of the quantization density in the scheme for quantifying the input directly. Hence if quantifying input with encoding-decoding scheme is used, the quantization density can be chosen to be slightly smaller under the network resource constraint. However, if quantifying the input without encoding-decoding scheme is used, μ should be set slightly bigger to produce better tracking performance. A comparison of the cost function values for different quantization schemes along the trials are shown in Fig. 10 with the quantization density $\mu = 0.8$. Under this measure, the encoding-decoding scheme has better performance than the scheme for quantifying the input without encoding-decoding scheme.

To examine the fault-tolerance performance, an actuator time-varying fault $\alpha = 0.9 + 0.1\sin(\pi t)$ is introduced on trial 15, and in this case $\|\Delta\alpha\| = 0.2$ from $\alpha = I + \Delta\alpha$. The parameters in the quantizer are chosen as $z_0 = 2$ and $\mu = 0.8$. In quantifying the input with encoding-decoding scheme, the values of K_u and K_e (not shown for ease of presentation) are obtained by setting the weighting parameters as $q = 80,000$, $r = 0.04$, $s = 0.0001$ and the condition (62) of Theorem 3 is satisfied. The condition of Theorem 4 for quantifying input without encoding-decoding scheme also holds in this case, and the results of simulating the controlled system over 30 trials are shown in Fig. 11, it can be seen that the norm of point-to-point tracking errors for two different quantization schemes can return to an acceptable value when the actuator fault occurs on trial 15.

6. Conclusion and future work

In this paper, the point-to-point ILC problem for linear discrete-time systems with quantized signals is considered under the general networked structure. To solve this problem, both the encoding-decoding mechanism and logarithmic quantizer are used

to develop a method of quantifying the designed NOILC inputs. It is shown that the encoding-decoding scheme can achieve accurate tracking effect despite the small quantization density. In addition, an extension to fault-tolerant design is developed and it is shown that a better actuator fault-tolerant performance can be achieved for quantifying the input with the encoding-decoding scheme. Finally, a numerical case study is given to illustrate the application of the designs.

The results from the numerical case study demonstrate the effectiveness of the new designs. These support further research to enable the full potential of these designs can be assessed. In general, these designs can be conservative, and further research is needed to reduce this effect.

References

Arimoto, S., Kawamura, S., & Miyazaki, F. (1984). Bettering operations of robots by Learning. *Journal of Robotic Systems, 1 (2)*, 123–140.

Bu, X., Wang, T., Hou, Z., & Chi, R. (2015). Iterative learning control for discrete-time systems with quantised measurements, *IET Control Theory Applications, 9 (9)*, 1455–1460.

Chen, Y., Chu, B., & Freeman, C. T. (2019). A coordinate descent approach to optimal tracking time allocation in point-to-point ILC, *Mechatronics, 59*, 25–34.

Chen, Y., Chu, B., & Freeman, C. T. (2019). Iterative learning control for robotic path following with trial-varying motion profiles, *IEEE/ASME Transactions on Mechatronics*, doi:10.1109/TMECH.2022.3164101.

Freeman, C. T., Cai, Z., Rogers, E., & Lewin, P. L. (2011). Iterative learning control for multiple point-to-point tracking application, *IEEE Transactions on Control Systems Technology, 19*, 590–600.

Freeman, C., Rogers, E., Hughes,A. M., Burridge,J., & Meadmore, K. (2012). Iterative learning control in health care: Electrical stimulation and robotic-assisted upper-limb stroke rehabilitation, *IEEE Control Systems Magazine, 32 (1)*, 18 –43.

Meadmre, K. L. and Hughes, A. M. and Freeman, C. T. and Cai, Z. and Tong, D. and Burridge, J. H. and Rogers, E. (2012). Functional electrical stimulation mediated by iterative learning control and 3D robotics reduces motor impairment in chronic stroke. *Neurorehabilitation and Neural Repair, 9 32*, 559–568.

Fu, M., & Xie, L. (2005). The sector bound approach to quantized feedback control, *IEEE Transactions on Automatic Control, 50 (11)*, 1698–1711.

Gao, M., Sheng, L., Zhou, D., & Gao, F. (2017). Iterative learning fault-tolerant control for networked batch processes with multirate sampling and quantization effects, *Industrial & Engineering Chemistry Research 56 (9)*, 2515–2525.

Huo, N., Shen, D. (2020). Encoding-decoding mechanism-based finite-level quantized iterative learning control with random data dropouts, *IEEE Transactions on Automation Science and Engineering, 17 (3)*, 1343–1360.

Jin, X. (2018). Iterative learning control for output-constrained nonlinear systems with input quantization and actuator faults, *International Journal of Robust and Nonlinear Control, 28 (2)*, 729–741.

Jin, X. (2018). Fault-tolerant iterative learning control for mobile robots non-repetitive trajectory tracking with output constraints, *Automatica, 94*, 63–71.

Johansen, S. V., Jenson, M. R., Chu, B., Bendsten, J. D., Mogensen, J., & Rogers, E. (2021). Broiler FCR optimization using norm optimal terminal iterative learning control, *IEEE Transactions on Control System Technology, 29 (2)*, 580–592.

Liu, X., Wei, S., & Chai, Y. (2020). An iterative learning scheme-based fault estimator design for nonlinear systems with quantised measurements, *Journal of the Franklin Institute, 357 (1)*, 606–621.

Oomen,T., & Rojas, C. R. (2017). Sparse iterative learning control with application to a

wafer stage: Achieving performance, resource efficiency, and task flexibility, *Mechatronics*, *47*, 134–147.

Owens, D. H. (2016). Iterative Learning Control An Optimization Paradigm, Springer.

Ratcliffe, J. D. (2004). Iterative learning control implemented on a multi-axis system, [Doctoral dissertation, University of Southampton, UK].

Shen, D., & Xu, Y. (2016). Iterative learning control for discrete-time stochastic systems with quantized information, *IEEE/CAA Journal of Automatica Sinica*, *3 (1)*, 59–67.

Shen, D., & Zhang, C. (2020). Zero-error tracking control under unified quantized iterative learning framework via encoding-decoding method, *IEEE Transactions on Cybernetics*, doi:10.1109/TCYB.2020.3004187.

Son, T. D., Ahn, H. S., & Moore, K. L. (2013). Iterative learning control in optimal tracking problems with specified data points, *Automatica*, *49 (5)*, 1465–1472.

Tao, H., Paszke, W., Rogers, E., Yang, H., & Galkowski, K. (2017). Iterative learning fault-tolerant control for differential time-delay batch processes in finite frequency domains, *Journal of Process Control*, *56*, 112–128.

Wang, L., Mo, S., Zhou, D., Gao, F., & Chen, X. (2012). Robust delay dependent iterative learning fault-tolerant control for batch processes with state delay and actuator failures, *Journal of Process Control*, *22 (7)*, 1273–1286.

Zhang, C., & Shen, D. (2018). Zero-error convergence of iterative learning control based on uniform quantization with encoding and decoding mechanism, *IET Control Theory & Applications*, *12 (14)*,1907–1915.

Zhou, C., Tao, H., Chen, Y., Stojanovic, V., & Paszke, W. (2022). Robust point-to-point iterative learning control for constrained systems: A minimum energy approach, *International Journal of Robust and Nonlinear Control*, doi:https://doi.org/10.1002/rnc.6354.

Zhuang, Z., Tao, H., Chen, Y., Stojanovic, V., & Paszke, W. (2022). Iterative learning control for repetitive tasks with randomly varying trial lengths using successive projection, *International Journal of Adaptive Control and Signal Processing*, *36 (5)*,1196–1215.